Supplementary information for

Local redox cycling-based electrochemical chip device with nanocavities for multi-electrochemical evaluation of embryoid bodies

Yusuke Kanno[1], Kosuke Ino[1], Hitoshi Shiku[1], and Tomokazu Matsue[1,2]

[1] Graduate School of Environmental Studies, Tohoku University, Japan

[2] WPI-Advanced Institute for Materials Research, Tohoku University, Japan

Corresponding authors:

Kosuke Ino (ino.kosuke@bioinfo.che.tohoku.ac.jp)

Tomokazu Matsue (matsue@bioinfo.che.tohoku.ac.jp)

Other substrates for electrochemical detection of ALP

Other substrates, such as L-ascorbic acid phosphate (AAP) [1] and *p*-nitrophenyl phosphate (PNPP) [2] are also commercially available. The difference in potentials for detection between the substrate and the enzymatic product is sufficient, so that the substrate and the enzymatic product can be electrochemically differentiated. However, these chemicals are unsuitable for the present system because these enzymatic products, L-ascorbic acid (AA) and *p*-nitrophenol (PNP), are unsuitable for redox cycling-based detection. Although ferrocene-derived substrates was reported,[3-5] these substrates are not commercially available, and some of them require electrode modification, which is time-consuming.

Evaluation of the etching process

The connection of electrodes to a digital voltmeter is shown in Fig. S1. Detailed discussion is shown in the main text.

Simulation model for redox cycling

The configurations of the model are shown in Figs. S2 and S3. Detailed discussion is shown in the main text.

Calibration curve for $FcCH_2OH$

The connection of electrodes to the potentiostat is shown in Fig. S4. Detailed discussion is shown in the main text.

Imaging process

The detailed scheme of the imaging process is shown in Fig. S5.

Simulation of electric field strength for DEP

Electric fields around electrodes were calculated using COMSOL Multiphysics (ver. 5.1; COMSOL Inc., USA). A three dimensional model was fabricated. The configuration of the model is shown in Fig. S6A. The model consists of a glass substrate, a SU-8 layer, a nanocavity, and top and bottom ring electrodes. The model is filled with a 0.2 M sucrose solution. The relative permittivity (ε_r) of the glass substrate, the SU-8 layer and the 0.2 M sucrose solution were set to 4.0, 3.3 and 78, respectively, according to the SU-8 3000 data sheet and the references.[6, 7] Opposite electrostatic potentials (effective value: ± 7.07 V) were applied to the ITO and ring electrodes. The cross-sectional image of the electric field strength was shown in Fig. S6B. In the near of the nanocavity, the electric field strength is over 1 kV/cm. When the distance from the inside wall of the microwell became large, the electric filed strength decreases dramatically.

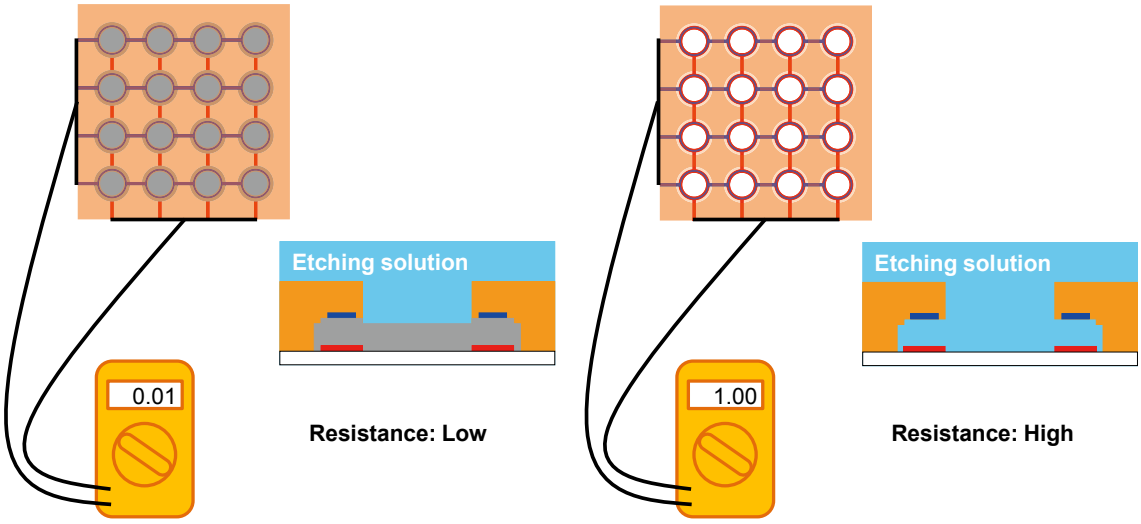

Figure S1

Connection of electrodes to a digital voltmeter for measurement of the resistance between the top and bottom electrodes to evaluate the etching process.

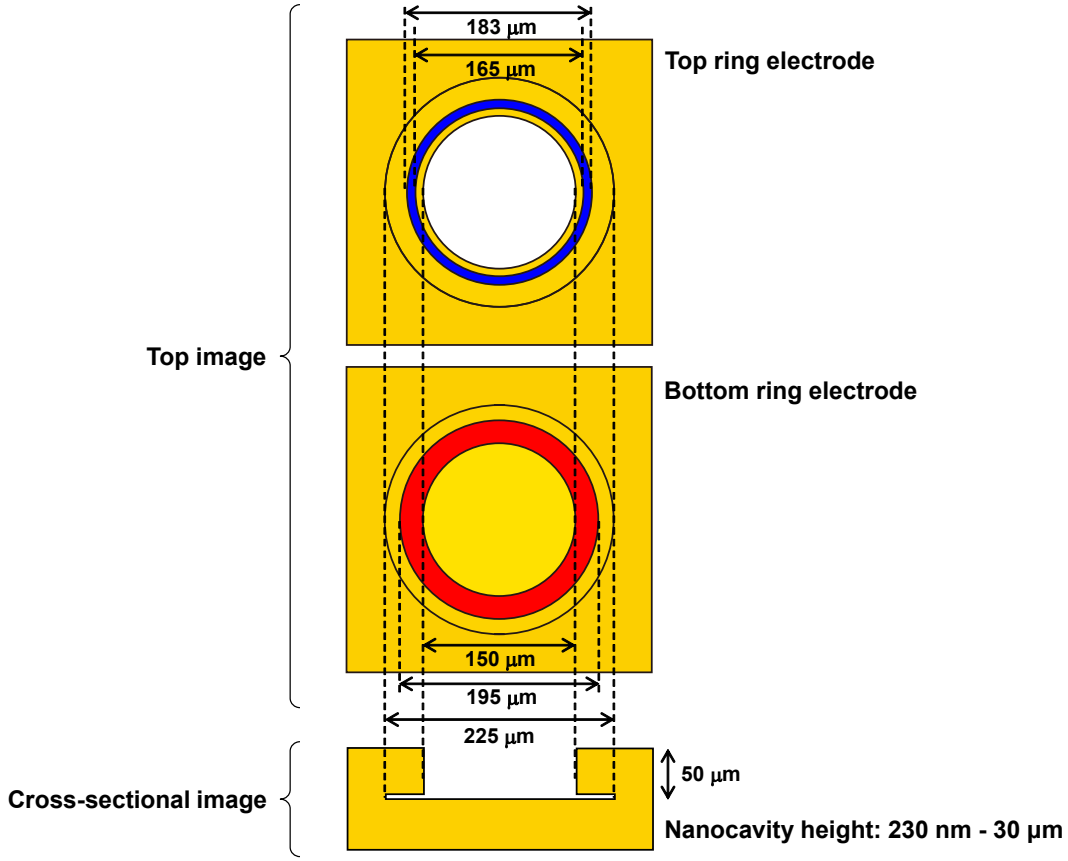

Figure S2

Configuration of the simulation model for redox cycling mode.

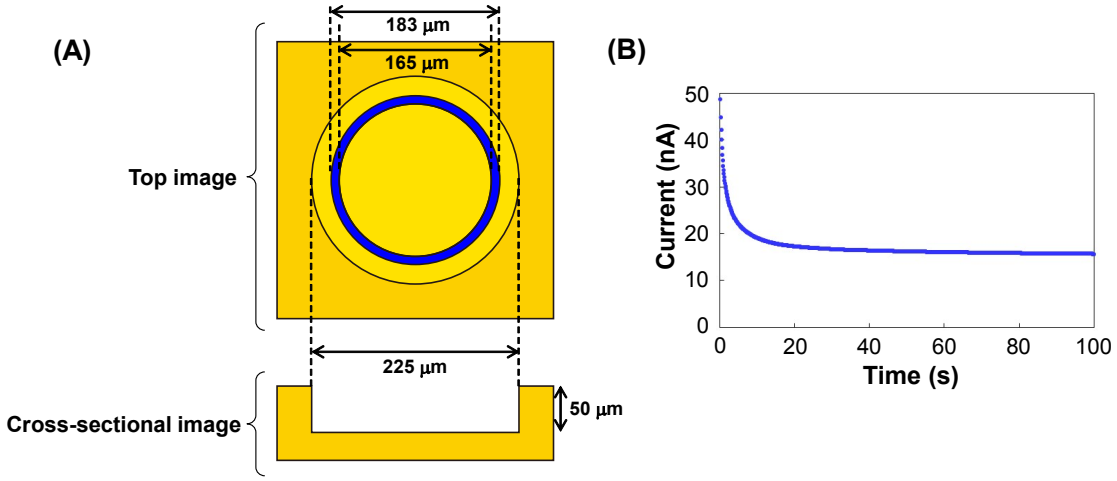

Figure S3

(A) Configuration of the model for simulation of non-redox cycling mode. (B) Chronoamperometry of 1.0 mM $FcCH_2OH$ at 0.50 V.

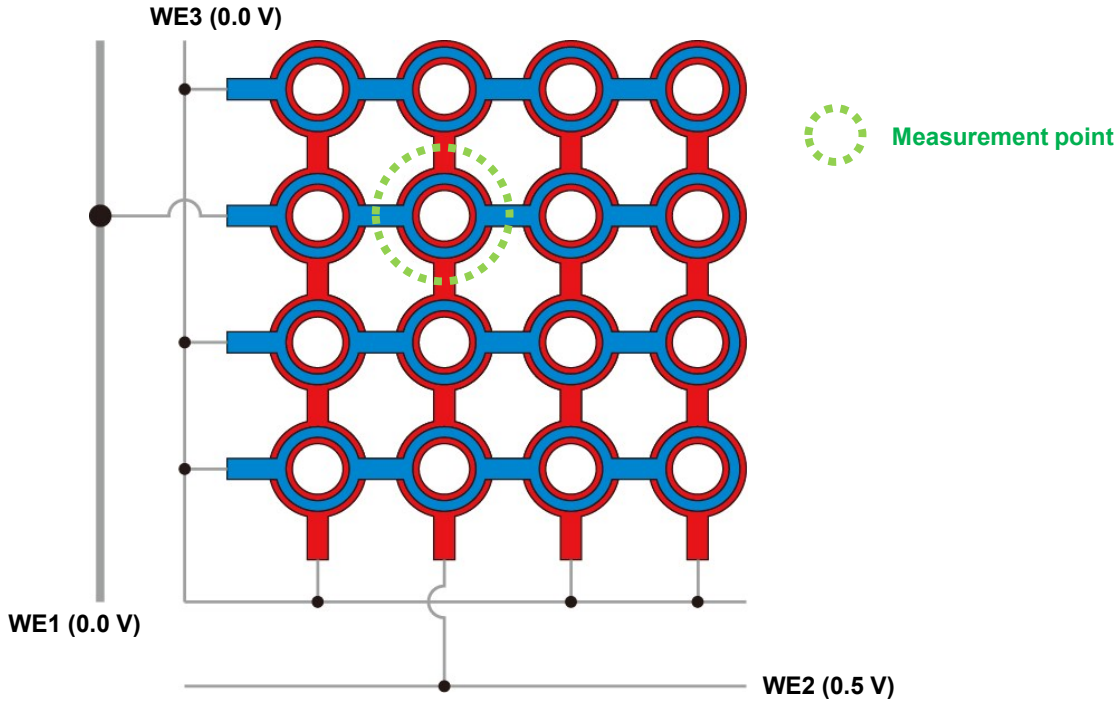

Figure S4

Connections of electrodes to the potentiostat for the calibration curve. Three working electrodes of a multichannel potentiostat (WE1, WE2 and WE3) were used for detection.[8-10] All electrodes were held at 0.00 V using WE3. The potential of a column electrode was stepped from 0.00 V to 0.50 V to oxidize ferrocenemethanol ($FcCH_2OH$) to $FcCH_2OH^+$ at the column electrode using WE2 and a switching matrix. The oxidation product, $FcCH_2OH^+$, was reduced back to $FcCH_2OH$ at the row electrodes. The reduction current of $FcCH_2OH^+$ at a row electrode was monitored through WE1 and the switching matrix. The reduction current indicated the redox cycling-based electrochemical signal from a single sensor.

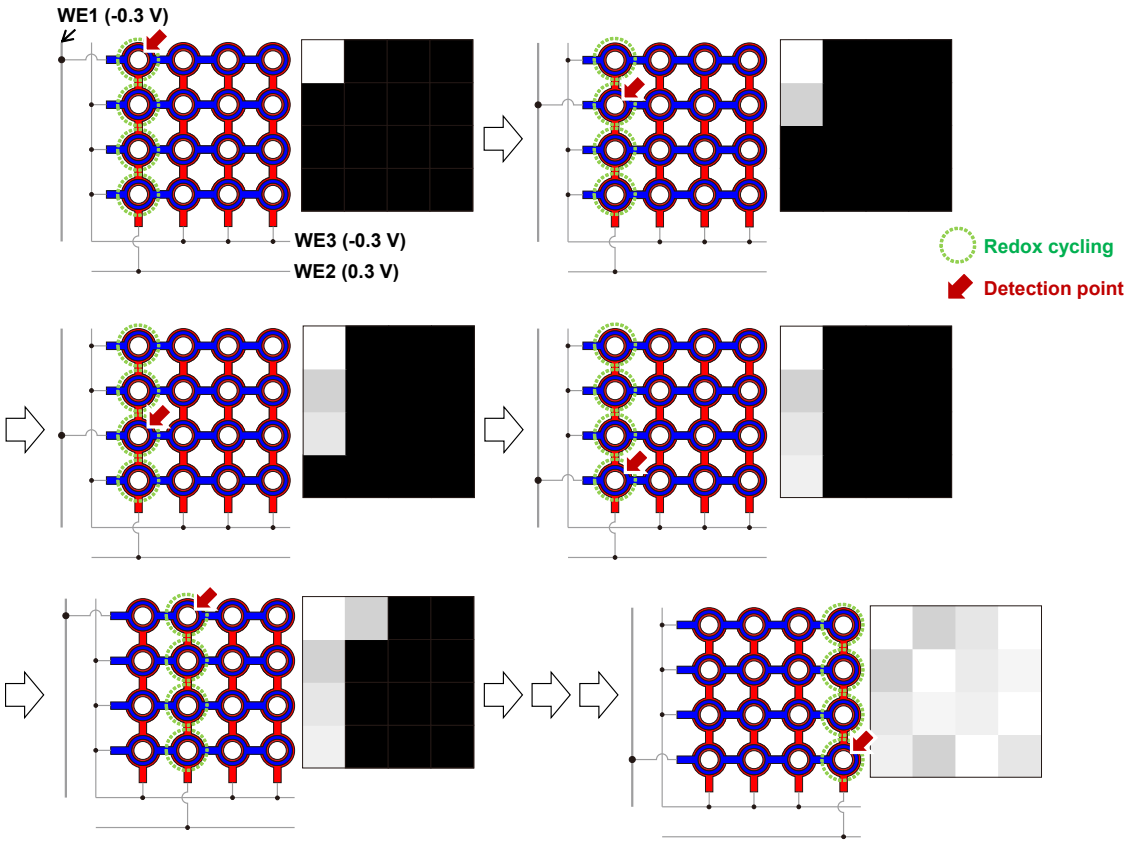

Figure S5

Imaging process for the detection of *p*-aminophenol (PAP) produced after alkaline phosphatase (ALP) reaction. A multichannel potentiostat consisting of three working electrodes (WE1, WE2, and WE3) was used for imaging.[8-10] The potentials of the row and column electrodes were controlled by changing the connection of the row and column electrodes to WE1, WE2, and WE3 through a switch matrix.[8-10] The row electrodes were used for potential control and data acquisition, and the column electrodes were used only for potential control. Arrows indicate a measurement point. Firstly, all electrodes were held at -0.30 V. The first column electrode was then stepped from -0.30 to 0.30 V to oxidize PAP to *p*-quinone imine (QI) only at the first column electrode. QI was then reduced back to PAP at the row electrodes. After current stabilization was achieved, the reduction current of QI at the first row electrode was acquired. By changing the electrodes using the switch matrix, the reduction current at the second row electrode was then acquired. After the responses at the first column electrode were acquired, the potential for the first column electrode was stepped back from 0.30 to -0.30 V, and the potential for the second column electrode was stepped from -0.30 to 0.30 V, so that the electrochemical signals at the sensor points of the second column electrode could be sequentially acquired. After electrochemical detection was completed, a 2D electrochemical image consisting of the electrochemical signals was constructed. The scanning process was performed automatically using a LabVIEW program.

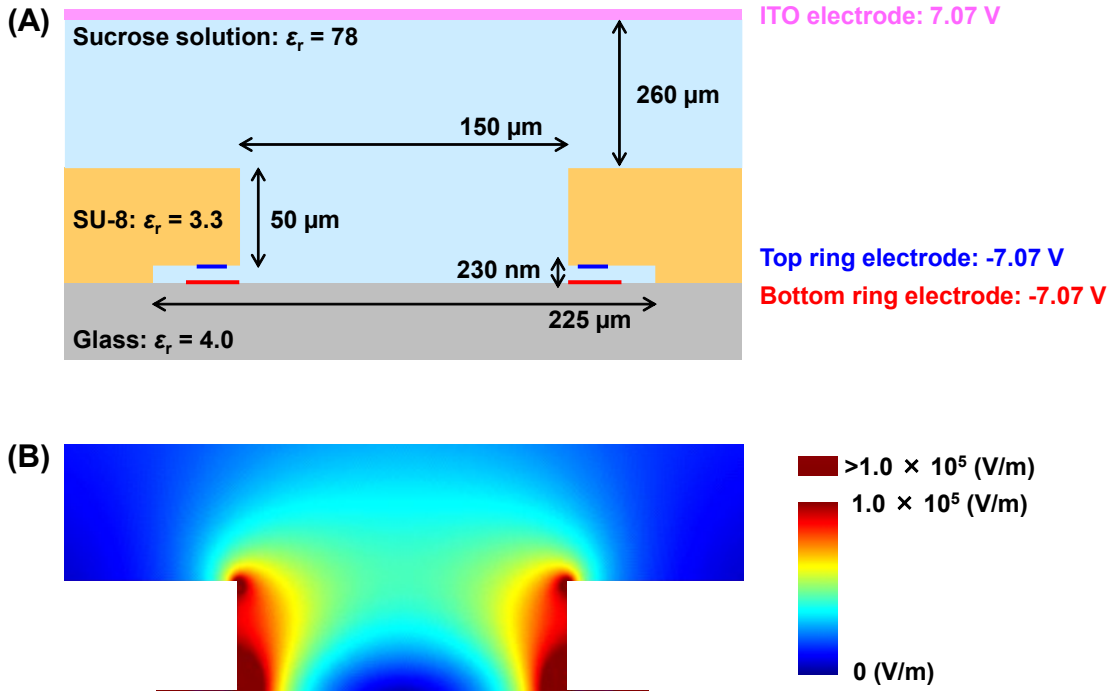

Figure S6

Simulation of electric field strength during DEP. (A) Configuration of the model (not to scale). (B) Cross-sectional image of electric field strength in the sucrose solution.

Movie S1

Device during etching of the sacrificial Cr layer described in Fig. 5. The movie is a 64 time-speed movie.

Movie S2

EBs during the DEP process shown in Fig. 9. The flow rate just after inducing flow was estimated to approximately 1.5 mm/s from the Movie S2.

References

1. S. Noh, D. T. Ha, H. Yang and M. S. Kim, *Analyst*, 2015, **140**, 3947-3952.
2. S. P. Ru, J. Wu, Y. B. Ying and F. Ji, *Chin. J. Anal. Chem.*, 2012, **40**, 835-839.
3. S. Goggins, C. Naz, B. J. Marsh and C. G. Frost, *Chem. Commun.*, 2015, **51**, 561-564.
4. K. Ino, Y. Kanno, T. Arai, K. Y. Inoue, Y. Takahashi, H. Shiku and T. Matsue, *Anal. Chem.*, 2012, **84**, 7593-7598.
5. B. Limoges and C. Degrand, *Anal. Chem.*, 1996, **68**, 4141-4148.
6. C. G. Akode, K. S. Kanse, M. P. Lokhande, A. C. Kumbharkhane and S. C. Mehrotra, *Pramana-J. Phys.*, 2004, **62**, 973-981.
7. C. Rosales and K. M. Lim, *Electrophoresis*, 2005, **26**, 2057-2065.
8. K. Ino, T. Nishijo, T. Arai, Y. Kanno, Y. Takahashi, H. Shiku and T. Matsue, *Angew. Chem., Int. Ed.*, 2012, **51**, 6648-6652.
9. K. Ino, Y. Kanno, T. Nishijo, T. Goto, T. Arai, Y. Takahashi, H. Shiku and T. Matsue, *Chem. Commun.*, 2012, **48**, 8505-8507.
10. K. Ino, W. Saito, M. Koide, T. Umemura, H. Shiku and T. Matsue, *Lab Chip*, 2011, **11**, 385-388.